Handout 5: magnetic fields during recombination

We have seen that the structure of the magnetic field is characterized by some simple principles. Its magnetic energy spectrum $E_{\rm M}(k)$ has a k^4 subinertial range up until some peak wavenumber $k_{\rm p}$. It is then followed by an inertial range, where either $E_{\rm M}\propto k^{-5/3}$ or perhaps slightly steeper $\propto k^{-2}$ (Brandenburg et al., 2015).

As time goes on, $k_{\rm p}$ decreases and is given by $k_{\rm p}=\xi_{\rm M}(t)^{-1}$, where $\xi_{\rm M}(t)\propto t^q$ follows a power law where the value of q obtained from dimensional arguments: $q=2/3$ when the mean magnetic helicity density, $I_{\rm M}=\langle\boldsymbol{A}\cdot\boldsymbol{B}\rangle$ is conserved, and $q=4/9$ when the Hosking integral, $I_{\rm H}$ is conserved. The spectrum evolves underneath an envelope $E_{\rm M}(k)\propto k^\beta$, where $\beta=0$ when $I_{\rm M}=$ const, and $\beta=3/2$ when $I_{\rm H}=$ const. The magnetic mean energy density is $\mathcal{E}_{\rm M}(t)=\int E_{\rm M}(k,t)\,{\rm d}k$ and it always decays like $\mathcal{E}_{\rm M}(t)\propto t^{-p}$, where $p=2/3$ when $I_{\rm M}=$ const and $p=10/9$ when $I_{\rm H}=$ const. In the diagnostic diagram, $v_{\rm A}(t)$ versus $\xi_{\rm M}(t)$, we have $v_{\rm A}\propto\xi_{\rm M}^{-\kappa}$, where where $\kappa=1/2$ when $I_{\rm M}=$ const, and $\kappa=5/4$ when $I_{\rm H}=$ const.

The evolution is approximately selfsimilar. This should should be true during the entire radiation-dominated era, which covers at least 24 orders of magnetitude, at least from the time of the electroweak era at $t_{\rm ph}\approx10^{-11}\,$s to the time of recombination at $t_{\rm ph}\approx370,000\,{\rm yr}\approx10^{13}\,$s. After that, we still have to cover 4.6 orders of magnitude to $t_{\rm ph}\approx13.8\,{\rm Gyr}\approx4\times10^{17}\,$s. So what does this mean for the magnetic field today? How much magnetic field will have survived and what is its length scale today? To answer these questions, we have to understand how the physics changes during this time and how this affects the inverse cascade behavior.

1 From a radiation fluid to a baryon fluid

An important change is that during the radiation-dominated era, the plasma was a radiation fluid where the pressure is $p=\rho_\gamma c_{\rm s}^3$ and $c_{\rm s}^2=c^2/3$. After that, radiation became dynamically unimportant and the plasma became a baryon fluid with the density $\rho_{\rm b}$. Also the time evolution of the scale factor changed from $a(t_{\rm ph})\propto t_{\rm ph}^{1/2}$ to $a(t_{\rm ph})\propto t_{\rm ph}^{2/3}$. However, during the process of recombination, the baryon fluid was still strongly coupled to the photons through photon drag and the momentum equation reads

$$\frac{\partial\boldsymbol{u}_{\rm ph}}{\partial t}=a^{3/2}\left[-(H+\alpha)\boldsymbol{u}_{\rm ph}-a^{-1}\boldsymbol{u}_{\rm ph}\cdot\boldsymbol{\nabla}\boldsymbol{u}_{\rm ph}-\frac{\boldsymbol{\nabla}\phi}{a}+\rho_{\rm b}^{-1}\left(-a^{-1}\boldsymbol{\nabla}p+\boldsymbol{J}_{\rm ph}\times\boldsymbol{B}_{\rm ph}+a^{-1}\boldsymbol{\nabla}\cdot2\rho_{\rm b}\nu\mathsf{S}_{\rm ph}\right)\right],\tag{1}$$

where $\alpha=4x_e\rho_\gamma\sigma_{\rm Th}/3m_pc$ is the photon drag relaxation rate with x_e being the ionization fraction, $\rho_\gamma c^2$ is the radiation energy density, $\sigma_{\rm Th}$ is the Thomson cross section, and m_p is the proton mass. The effects of this drag were already studied by Banerjee & Jedamzik (2004), and especially in recent times in attempts to alleviate the Hubble tension (Jedamzik & Pogosian, 2020; Jedamzik et al., 2021, 2025).

2 Effect of drag on the diagnostic diagram

What happens when drag is turned on during a short interval, but then turned off again? The answer is—surprisingly—not much!

We use the 2-D run 2m6 of BNV24 as reference run. It has a resolution of 16384^2 meshpoints and a magnetic Prandtl number of 10. We add a drag term $-\alpha\boldsymbol{u}$ to the momentum equation, but keep it on only for a certain time interval. Figure 1 shows the effect on the Lundquist number and the parameter $\tilde{C}_{\rm M}=v_{\rm A}t/\xi_{\rm M}$. After some excursion, both values seem to return to the original track. Figure 2 shows that by $t=100$ and 200, the evolution is back on track!

In 2-D, we expect $\xi_{\rm M}\sim t^{1/2}$ and $v_{\rm A}\sim t^{-1/2}$. Therefore, we expect Lu = const and $v_{\rm A}t/\xi_{\rm M}=$ const. We see that, when drag is acting, Lu $\propto v_{\rm A}\xi_{\rm M}$ increases, and when it is off again, it decreases. Figure 3

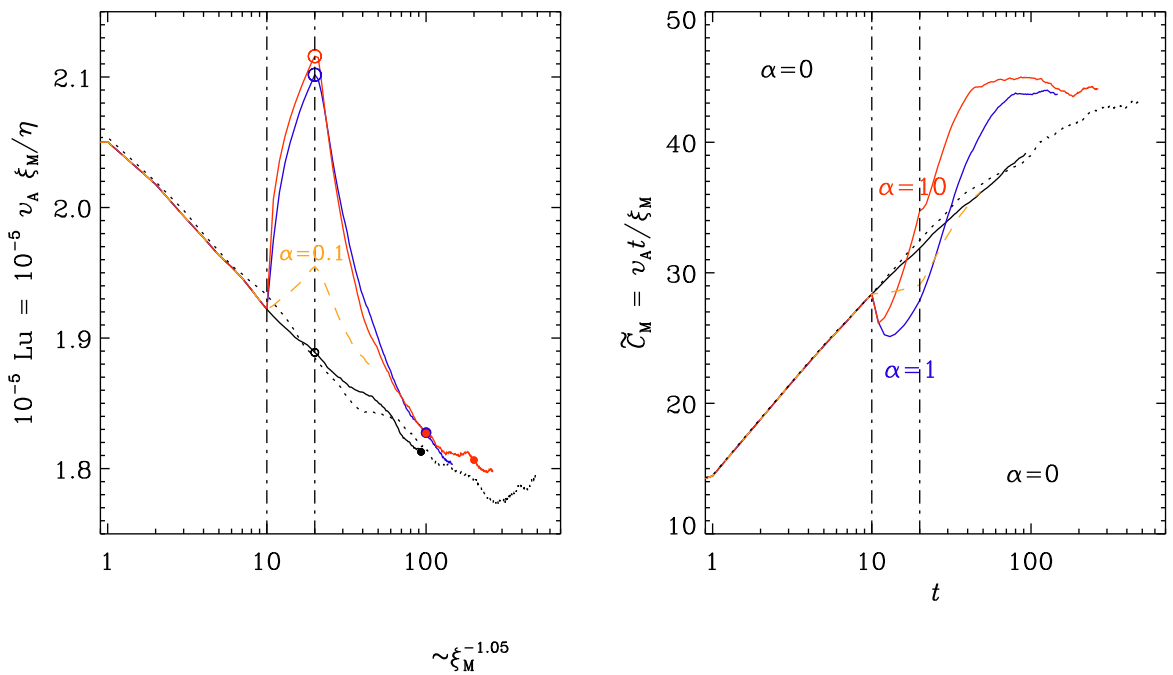

Figure 1: Two versions of useful compensated plots showing time dependences of $\mathrm{Lu} = v_\mathrm{A}\xi_\mathrm{M}/\eta$ (scaled by 10^{-5}) and $\tilde{C}_\mathrm{M} = v_\mathrm{A}t/\xi_\mathrm{M}$. In both panels, the dotted lines apply to an initial condition with a different set of random phases compared to the run shown as black lines.

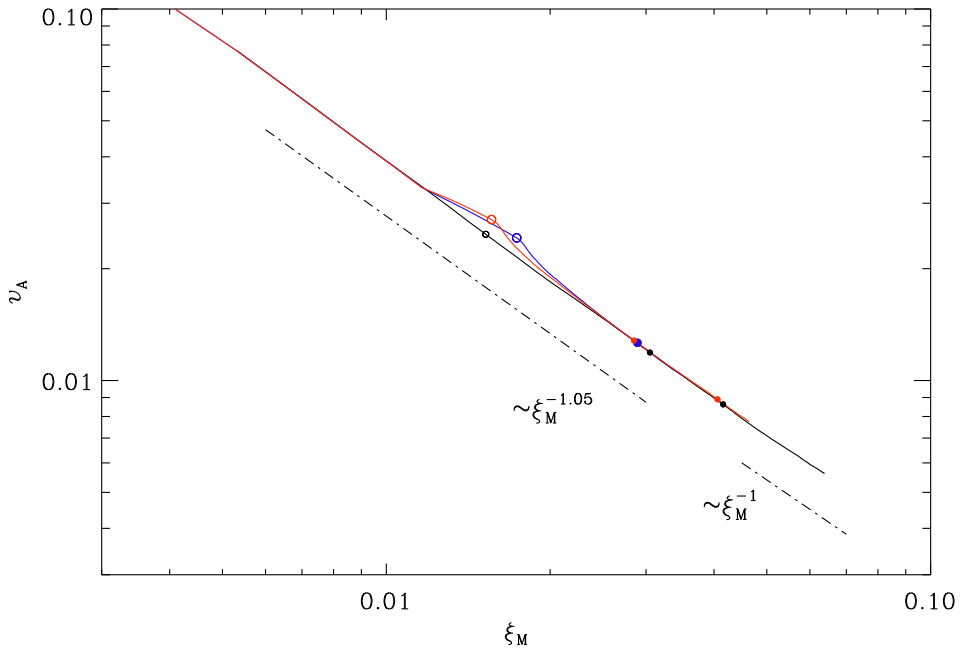

Figure 2: Diagnostic diagram showing Run 2m6 of BNV24 in black, and runs with $\alpha = 1$ (blue) and 10 (red) being turned on during $10 \le t \le 20$. The open symbols denote the times $t = 20$ when the drag is turned off again. The filled symbols denote the times 100 and 200. In 2-D, we expext $v_\mathrm{A} \propto \xi_\mathrm{M}^{-1}$.

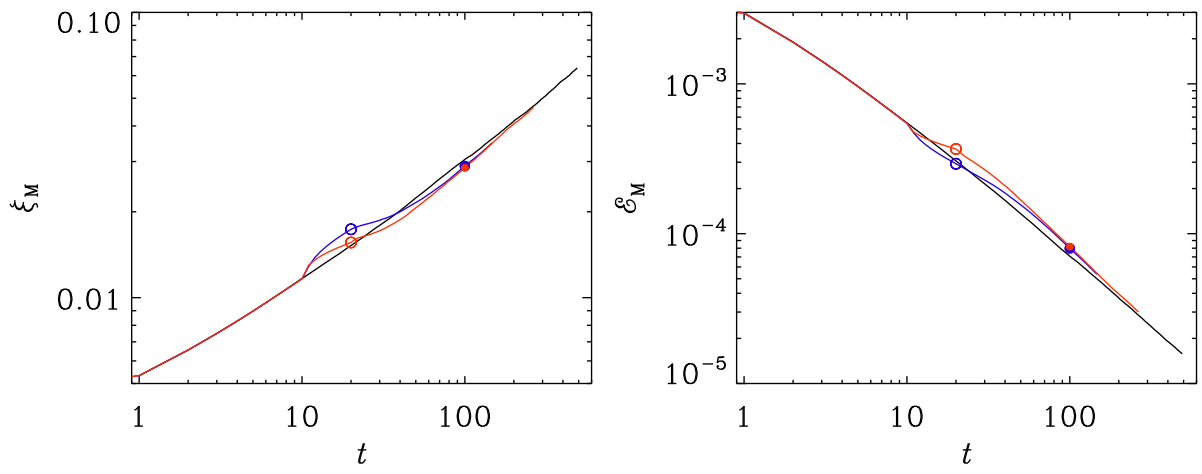

Figure 3: Time dependences of ξ_M and $\mathcal{E}_M$.

shows that, when drag is acting, ξ_M increases by more than the amount by which v_A decreases. This explains why $\mathrm{Lu} \propto v_A \xi_M$ increases. When drag is off again, v_A falls off less rapidly and ξ_M increases less rapidly. This explains why $\mathrm{Lu} \propto v_A \xi_M$ decreases again.

3 Change of the scale factor

During the transition from radiation to matter domination, there are many different changes to the magnetic field evolution: the electrons, and thereby also the baryons, gradually decouple from the photon fluid, so the magnetic field is no longer controlled by radiation, but by the gas motions. Furthermore, the degree of ionization and other thermodynamic quantities changed with time. Also, of course, the temporal dependence of the scale factor of the Universe changed. These effects have been incorporated in studies of primordial magnetic field evolution (Jedamzik et al., 2025). An important motivation for such studies is the fact that around the time of recombination, magnetic fields may have led to significant density fluctuations that increased the recombination rate and lowered the sound horizon. This, in turn, might have led to a smaller Hubble parameter at that time, which would alleviate the Hubble tension (Jedamzik & Pogosian, 2020).

The strong damping of the fluid motions would stop the inverse cascade. After the end of the recombination epoch, however, when the plasma has decoupled from the radiation, the electric conductivity is still large enough for the magnetic field to interact with the gas. One therefore expects the inverse cascade to resume. The study of its continued evolution is important for setting the stage for detailed low-redshift simulations (**?**).

Simulations of the matter-dominated low-redshift universe are usually performed using supercomoving coordinates (Jedamzik et al., 2025), where the conformal time is given by

$$t_n = \int \mathrm{d}t_{\mathrm{ph}}/a^n \tag{2}$$

with either $n = 2$ (Martel & Shapiro, 1998), $n = 3/2$ (Banerjee & Jedamzik, 2004; Jedamzik et al., 2025), as opposed to $n = 1$ for the usual comoving coordinates. The subscript 'ph' indicates physical variables and is sometimes also applied as a superscript. In the two cases with $n = 2$ and $n = 3/2$, the momentum equation has a term that depends on $a(t_n)$. In the first case, there is an $a(t_n)$ factor in front of the Lorentz force, while in the second case there is a modified Hubble drag term. In addition, the comoving velocity is different: $\boldsymbol{u}_2 = a(t_2)\,\boldsymbol{u}_{\mathrm{ph}}$ for $n = 2$ and $\boldsymbol{u}_{3/2} = a^{1/2}\,\boldsymbol{u}_{\mathrm{ph}}$ for $n = 3/2$, as opposed to $\boldsymbol{u}_1 = \boldsymbol{u}_{\mathrm{ph}}$

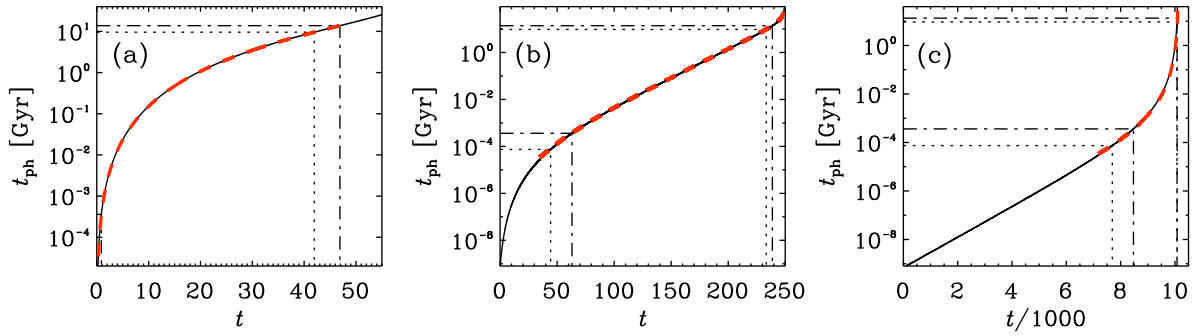

Figure 4: Dependence of $t_{\rm ph}$ on t_n for (a) $n = 1$, (b) $n = 3/2$, and (c) $n = 2$, obtained by solving Equation (5) with $\Omega_{\rm rad} = 10^{-4}$ and $\Omega_\Lambda = 0.73$, as well well as $H_0 = 0.0692\,{\rm Gyr}^{-1} \approx 0.71\,{\rm km/s\,kpc}^{-1}$. The dashed-dotted lines denote $z = 1100$ at $t_{\rm ph} = 370,000\,{\rm yr}$ and $z = 0$ at $t_{\rm ph} = 13.8\,{\rm Gyr}$, while the dotted lines denote $a = 3.7 \times 10^{-4}$ at $t_{\rm ph} = 7.4 \times 10^{-5}\,{\rm Gyr}$ and $a = 0.72$ at $t_{\rm ph} = 9.6\,{\rm Gyr}$.

for $n = 1$. Thus, we can capture all three cases by writing

$$\boldsymbol{u}_n = a^{n-1}\,\boldsymbol{u}_{\rm ph}. \tag{3}$$

Furthermore, in all three cases, the comoving magnetic field is given by $\boldsymbol{B} = a(t_n)^2\,\boldsymbol{B}_{\rm ph}$. Therefore, the comoving $\boldsymbol{B}$ is the same for all values of n, so it does not need to carry the subscript n. The scale factor $a(t_n)$ is the same regardless of whether the physical or conformal times are used, and what the value of n is.

The comoving baryon density $\rho_{\rm b}$ is given by $\rho_{\rm b} = a(t_n)^3\,\rho_{\rm b}^{\rm ph}$, while in the third case only the comoving radiation energy density ρ_γ is modeled and it is related to the physical one via $\rho_\gamma = a(t_n)^4 \rho_\gamma^{\rm ph}$. In the radiation-dominated era, we have $\rho_\gamma^{\rm ph} > \rho_{\rm b}^{\rm ph}$, so the evolution of baryons can be neglected, while in the matter-dominated era we have $\rho_\gamma^{\rm ph} < \rho_{\rm b}^{\rm ph}$, and the radiation can be neglected.

In principle, one should solve for both $\rho_{\rm b}$ and ρ_γ, as well as their corresponding velocities, which are mutually coupled through photon drag. Photon drag is particularly important around the time of recombination. The energy density of the primordial magnetic field may well exceed the thermal energy density of the baryons, which can lead to strongly supersonic motions with significant local density enhancements, as already mentioned above. Those are also referred to as baryon clumps (Jedamzik et al., 2025) and are of interest for alleviating the Hubble tension (Jedamzik & Pogosian, 2020).

Not much is known about the magnetic field evolution for the two variants of supercomoving coordinates. Both describes the same same physics, so the inverse cascade of the magnetic field should be exactly the same same. However, numerical effects such as the changing effective resolution may affect the result. This was recently demonstrated in studies of gravitational collapse using supercomoving coordinates with $n = 2$ (Brandenburg & Ntormousi, 2025).

Here, we want to study and compare the effects caused by the different comoving coordinate systems with $n = 3/2$ and $n = 2$. The two coordinate systems apply to arbitrary time dependencies of $a(t_n)$. To isolate this comparison from other complications, we will assume conditions where the fluid motions are always subsonic and no photon drag is present. This allows us to focus on possible effects on the inverse cascade behavior.

We note in passing that Martel & Shapiro (1998) also discuss a variant of comoving coordinates in which the magnetic field scales differently with $a(t_n)$, but this variant, which implies an anti-drag term in the induction equation, will not discussed in the present paper. The differences in the momentum equation will be discussed below.

4 Superconformal coordinates

As discussed in the introduction, superconformal coordinates are defined through $\mathrm{d}t = \mathrm{d}t_{\rm ph}/a^n$, where $n = 3/2$ (Banerjee & Jedamzik, 2004) or $n = 2$ (Martel & Shapiro, 1998) and $t_{\rm ph}$ is the physical (or cosmic) time. To obtain $a(t_n)$, we assume a standard ΛCDM universe and integrate $\mathrm{d}\ln a/\mathrm{d}t_{\rm ph} = H(a)$, where

$$H(a) = H_0\sqrt{\Omega_{\rm rad}/a^4 + \Omega_{\rm mat}/a^3 + \Omega_\Lambda} \tag{4}$$

is the prescribed dependence of the Hubble parameter on $a(t_n)$. We work with conformal time t, use $\mathrm{d}/\mathrm{d}t_{\rm ph} = a^{-n}\mathrm{d}/\mathrm{d}t$, and integrate to obtain $t_{\rm ph}(t_n)$ and $a(t_n)$, i.e.,

$$\frac{\mathrm{d}t_{\rm ph}}{\mathrm{d}t} = a^n \quad \text{and} \quad \frac{\mathrm{d}\ln a}{\mathrm{d}t} = a^n H(a). \tag{5}$$

To obtain the initial conditions for early times, we consider the limit $a \to 0$, so Equation (4) becomes $H(a) = H_0\Omega_{\rm rad}^{1/2}/a^2$. We then integrate $t_{\rm ph} = \int \mathrm{d}a/(aH)$, which yields $t_{\rm ph} = a^2/(2H_0\Omega_{\rm rad}^{1/2})$, i.e., $a = (2H_0\Omega_{\rm rad}^{1/2}t_{\rm ph})^{1/2}$. This relation is independent of n, but assumes that we start at a redshift that is well in the radiation-dominated era. Here we consider the initial redshifts $z_* = 4500$, the value also considered by Jedamzik et al. (2025), and $z_* = 10^6$. Thus, we solve Equation (5) with the initial conditions

$$a = a_* \equiv 1/(1+z_*), \quad t_{\rm ph} = t_{\rm ph}^* \equiv a_*^2/(2H_0\Omega_{\rm rad}^{1/2}). \tag{6}$$

In our three-dimensional hydromagnetic simulations, the comoving time step δt is governed by the usual Courant–Friedrich–Levy condition $\delta t \le C_{\rm CFL}\delta x/U_{\max}$, where $U_{\max}$ is the maximum propagation speed of all the wave modes that are present in the simulation. In the present case, $U_{\max}$ is mostly controlled by the sound speed c, but also the magnetic field enters through the Alfvén speed $v_{\rm A}$ and the fluid motions through $|\boldsymbol{u}|$.

In Figure 4, we compare the dependence of $t_{\rm ph}(t_n)$ for $n = 2$, 3/2, and 1 using $z_* = 4500$ and 10^6 and a constant time step. The range $10^3 \ge a(t_n) \ge 1$, corresponding to the time interval from recombination to the present time, $t_{\rm pres}$, is marked by dashed-dotted lines. We see that the dependence $t_{\rm ph}(t_n)$ is concave for $n = 2$ and convex for $n = 1$, but approximately linear for $n = 3/2$. This indicates that the exponent $n = 3/2$ distributes the instantaneous change in $t_{\rm ph}(t_n)$ approximately uniformly over the interval from recombination to $t_{\rm pres}$.

We recall that in all cases, our initial conformal time is always zero. However, when comparing $t_{\rm ph}(t_n)$ for different initial redshifts, we can make the curves overlap by adding a suitable offset $t_n(0)$ to $t_n \to t_n + t_n(0)$ for the runs with the smaller initial redshift. We see that the curves for $z_* = 4500$ and 10^6 overlap well, although there is a very small difference at the very beginning of the runs with $z_* = 4500$ relative to those with $z_* = 10^6$.

4.1 Governing equations

Both in the supercomoving as well as the ordinary comoving coordinates, the continuity and uncurled induction equations are the same as those in physical coordinates, i.e., we have

$$\mathrm{D}\ln\rho_{\rm b}/\mathrm{D}t_n = -\boldsymbol{\nabla}\cdot\boldsymbol{u}_n, \tag{7}$$

$$\partial\boldsymbol{A}/\partial t_n = \boldsymbol{u}_n \times (\boldsymbol{B} + \boldsymbol{B}_0) + \eta_n\nabla^2\boldsymbol{A}, \tag{8}$$

where $\mathrm{D}/\mathrm{D}t_n = \partial/\partial t_n + \boldsymbol{u}_n\cdot\boldsymbol{\nabla}$ is the advective derivative and $\boldsymbol{B} = \boldsymbol{\nabla}\times\boldsymbol{A}$ is the departure of the magnetic field from a uniform imposed field $\boldsymbol{B}_0$ that is applied in a few cases for test purposes. It is only the momentum equation where the scale factor $a(t_n)$ and/or its time derivative, $H = \mathrm{d}\ln a/\mathrm{d}t_{\rm ph}$, appear. For $n = 3/2$, this equation takes the form (Banerjee & Jedamzik, 2004)

$$\begin{aligned}\frac{\mathrm{D}\boldsymbol{u}_{3/2}}{\mathrm{D}t_{3/2}} &= -c_{3/2}^2\boldsymbol{\nabla}\ln\rho_{\rm b} - (\alpha_{3/2} + \tfrac{1}{2}\tilde{H})\boldsymbol{u}_{3/2} \\ &+ \rho_{\rm b}^{-1}\left[\boldsymbol{J}\times(\boldsymbol{B}+\boldsymbol{B}_0) + \boldsymbol{\nabla}\cdot(2\nu_{3/2}\rho_{\rm b}\mathsf{S}_{3/2})\right],\end{aligned} \tag{9}$$

where S_n is the rate-of-strain tensor with the components $\mathsf{S}^n_{ij} = (\partial_i u^n_j + \partial_j u^n_i)/2 - \delta_{ij}\boldsymbol{\nabla}\cdot\boldsymbol{u}_n/3$, and n is applied as a superscript when the vector components are already indicated by a subscript. Here, $\boldsymbol{J} = \boldsymbol{\nabla}\times\boldsymbol{B}/\mu_0$ is the current density and μ_0 is a vacuum permeability. Note that the viscosity term involving ν_n for $n = 3/2$ was not included in the original work of Banerjee & Jedamzik (2004). In Equation (9), we have both a physical drag term α and a Hubble drag term $\tilde{H} = a^{3/2}H$.

In Equation (9), the comoving sound speed is modified and given by

$$c_n = a^{n-1}\,c_{\rm ph}. \tag{10}$$

Thus, for $n > 1$, c_n would increase with time if $c_{\rm ph}$ were constant. In reality, $c_{\rm ph}$ is not constant. A reasonable approximation is to assume that $c^2_{\rm ph}$ is proportional to the temperature and thereby to a^{-1}. Thus, if instead $a^{-1}\,c^2_{\rm ph} = {\rm const}$, then also $c^2_{3/2} = a^{2n-3}\,c^2_{\rm pres} = {\rm const}$. This is also what will be assumed in the following, where $c_{\rm pres} \equiv c_{\rm ph}(t_{\rm pres})$.

A relation similar to Equation (10), but between the physical and kinematic viscosities is given by

$$\nu_n = a^{n-2}\nu_{\rm ph}, \tag{11}$$

and similarly for the magnetic diffusivity, $\eta_n = a^{n-2}\eta_{\rm ph}$.

For $n = 2$, the momentum equation takes the form (**?**Martel & Shapiro, 1998), i.e.,

$$\begin{aligned}\frac{{\rm D}\boldsymbol{u}_2}{{\rm D}t_2} &= -c_2^2\boldsymbol{\nabla}\ln\rho_{\rm b} - \alpha_2\boldsymbol{u}_2 \\ &\quad +\rho_{\rm b}^{-1}\left[a(t_n)\,\boldsymbol{J}\times(\boldsymbol{B}+\boldsymbol{B}_0) + \boldsymbol{\nabla}\cdot(2\nu_2\rho_{\rm b}\mathsf{S}_2)\right],\end{aligned} \tag{12}$$

so there is no Hubble drag. Instead, there is now an $a(t_n)$ factor in front of the Lorentz force.

More generally, for any value of n, we can write

$$\begin{aligned}\frac{{\rm D}\boldsymbol{u}_n}{{\rm D}t_n} &= -c_n^2\boldsymbol{\nabla}\ln\rho_{\rm b} - (\alpha_n + H_n)\boldsymbol{u}_n \\ &\quad +\rho_{\rm b}^{-1}\left[a^{2n-3}\,\boldsymbol{J}\times(\boldsymbol{B}+\boldsymbol{B}_0) + \boldsymbol{\nabla}\cdot(2\nu_n\rho_{\rm b}\mathsf{S}_n)\right],\end{aligned} \tag{13}$$

where $H_n = (2-n)\,a^nH$, so it vanishes for $n = 2$, wile for $n = 3/2$, the $a(t_n)$ term in front of the Lorentz force becomes unity. Alfvén speed is also modified by the a^{2n-3} factor in front of the Lorentz force and is thus $v_{\rm A}^{(n)} = a^{n-3/2}B_{\rm rms}/\sqrt{\rho_{\rm b}}$.

If we want to compare runs with different values of n and the same physical sound speed, an additional factor with a certain power of $a(t_n)$ would enter. In fact, it is the same prefactor as in front of the Lorentz force in Equation (13), which is unity for $n = 3/2$.

Note that for $n < 3/2$, the factor a^{2n-3} in the effective Lorentz force is larger than unity when $a \ll 1$, i.e., at very early times. This could imply that for $n < 3/2$, a certain magnetic field produces a large feedback on the flow at early times when $a \ll 1$. However, as discussed just above, the effective sound speed is also larger, so the magnetic feedback on the flow is actually the same same as for other value of n.

We recall that the effective comoving viscosity is $\nu_n = a^{n-2}\nu_{\rm ph}$. At early times, it is much larger than $\nu_{\rm ph}$ if $n < 2$. If we want to maintain the same physical viscosity and magnetic diffusivity, we must keep ν_n/a^{n-2} and η_n/a^{n-2} unchanged. Therefore, to reproduce an $n = 3/2$ run with constant $\nu_{3/2} = \eta_{3/2}$, we would need to set $\nu_n = a^{n-3/2}\nu_{3/2}$ and $\eta_n = a^{n-3/2}\nu_{3/2}$, i.e., the viscosity and magnetic diffusivity can be smaller in the beginning of the simulation. This agrees with our initial experience.

4.2 Transformation to physical coordinates

We have $\boldsymbol{x}_{\rm ph} = \boldsymbol{x}a(t_n)$, $k_{\rm ph} = k/a(t_n)$, $\boldsymbol{B}_{\rm ph} = \boldsymbol{B}/a^2$, $E^{\rm ph}_{\rm M}(k_{\rm ph}) = E_{\rm M}(k)/a^3$. Since $\langle\boldsymbol{B}^2_{\rm ph}\rangle/2 = \int E^{\rm ph}_{\rm M}(k_{\rm ph})\,{\rm d}k_{\rm ph} = \int E_{\rm M}(k)\,{\rm d}k/a^4 = \langle\boldsymbol{B}^2\rangle/2a^4$, this scaling obeys the expected a^{-4} scaling of the physical magnetic energy density (in the absence of turbulence).

The physical density is related to the comoving one via $\rho_{\rm b}^{\rm ph}=\rho_{\rm b}/a^3$, and therefore the physical Alfvén velocity, $v_{\rm A}^{\rm ph}=B_{\rm rms}^{\rm ph}/(\mu_0\rho_0^{\rm ph})^{1/2}$, is related to the comoving one via $v_{\rm A}^{\rm ph}=v_{\rm A}^{(n)}/a^{1/2}$. However, in view of the a–dependent term in front of the Lorentz force, the comoving Alfvén velocity is proportional to $a^{n-3/2}$. Therefore, the scaling of $v_{\rm A}$ agrees with those of c_n and $\boldsymbol{u}_n$; see Equation (3).

4.3 Numerical solutions

We perform numerical simulations using the Pencil Code (**?**). The modifications in Equation (13) can be invoked by using the module `SPECIAL=special/Lambda_CDM`. For most of our three-dimensional simulations, we use a resolution of 1024^3 meshpoints.

4.4 Tests

Given that we adopt periodic boundary conditions for all physical fields, the case of Alfvén waves is somewhat unusual, because there must be an imposed field that must then be treated as a given, time-dependent quantity. Thus, we work with $\boldsymbol{B}\to\boldsymbol{B}_0+\boldsymbol{\nabla}\times\boldsymbol{A}$, where $\boldsymbol{A}$ is periodic. In that case, $\boldsymbol{B}_0$ enters on the right-hand side of Equations (8)–(12) and Equation (13).

5 Sound waves

To simulate sound waves, we use as initial conditions $\ln\rho={\rm Ma}_0\sin kx$ and $u_{3/2}={\rm Ma}_0\sin kx$. We assume that $c_{3/2}={\rm const}=1\,{\rm km/s}$, which means that $c_{\rm s0,ph}=a\times1\,{\rm km/s}$, i.e., $c_{\rm s0,ph}=10^3\,{\rm km/s}$ at our initial value of $a=10^{-6}$.

In Figure 5, we compare the evolution of those sound waves in a space-time diagram of $u_{\rm ph}(t_{\rm ph},x_{\rm ph})$ for $n=3/2$ and $n=2$ with $k=0.5\,{\rm kpc}^{-1}$ in both cases. This results in about 15 oscillations during the matter-dominated epoch. The Mach number is 10^{-3}, and since $c_{3/2}={\rm const}=1\,{\rm km/s}$, we used $u_{3/2}^0=10^{-3}\,{\rm km/s}$ for $n=3/2$ and $u_2^0=10^{-6}\,{\rm km/s}$ for $n=2$.

We use $u_0=0.1\,c_{3/2}$, which is already large enough so that the sound wave steepens to develop a shock after a finite time. To dissipate this shock, we use a viscosity $\nu_{3/2}=10^{-4}$. For $n=2$, we use $\nu=a^{1/2}\nu_{3/2}$.

We define the matter dominated phase as the inverval when $\Omega_{\rm mat}/[a^3\,(H/H_0)^2]$ exceeds the value 1/2. Prior to that, the expansion of the universe is dominated by radiation, so $\Omega_{\rm rad}/[a^4\,(H/H_0)^2]>1/2$, and after that by the Λ term, i.e., $\Omega_\Lambda/(H/H_0)^2>1/2$. The corresponding values of $t_{\rm ph}$ are $7.4\times10^{-5}\,{\rm Gyr}$ and $9.6\,{\rm Gyr}$.

During the matter-dominated era, $a(t_{\rm ph})\propto t_{\rm ph}^{2/3}$. Thus, for $n=3/2$, we have $t_{3/2}=H_0^{-1}\ln t_{\rm ph}$, where $H_0^{-1}\approx13.8\,{\rm Gyr}$ is the age of the universe. During the time interval from $7.4\times10^{-5}\,{\rm Gyr}$ to $9.6\,{\rm Gyr}$, the value of $\log_{10}t_{\rm ph}$ changes by about 5.1 (from -4.1 to $+1$). With $c_{3/2}=1\,{\rm km/s}$ and $k=0.5\,{\rm kpc}^{-1}$, we have $c_{3/2}k_{3/2}\approx0.5\,{\rm Gyr}^{-1}$, so the period of sound waves is about $13\,{\rm Gyr}$. This corresponds to about $5.1/13=0.4$ oscillations.

6 Inverse cascade

In Figure 7, we compare the results for $n=3/2$ and $n=2$. The magnetic field is fully helical, so the spectra should have the same height in the radiation-dominated epoch. Note also that the conformal sound speed is always assumed to be constant in time.

Since $a=1$ at the present time $t_{\rm pres}=13.8\,{\rm Gyr}$, and since our length unit is kpc, our initial choice for the size of the domain of $(2\pi)^3$ corresponds to $(\approx6\,{\rm kpc})^3$. This is not much, and therefore we have also considered larger domains.

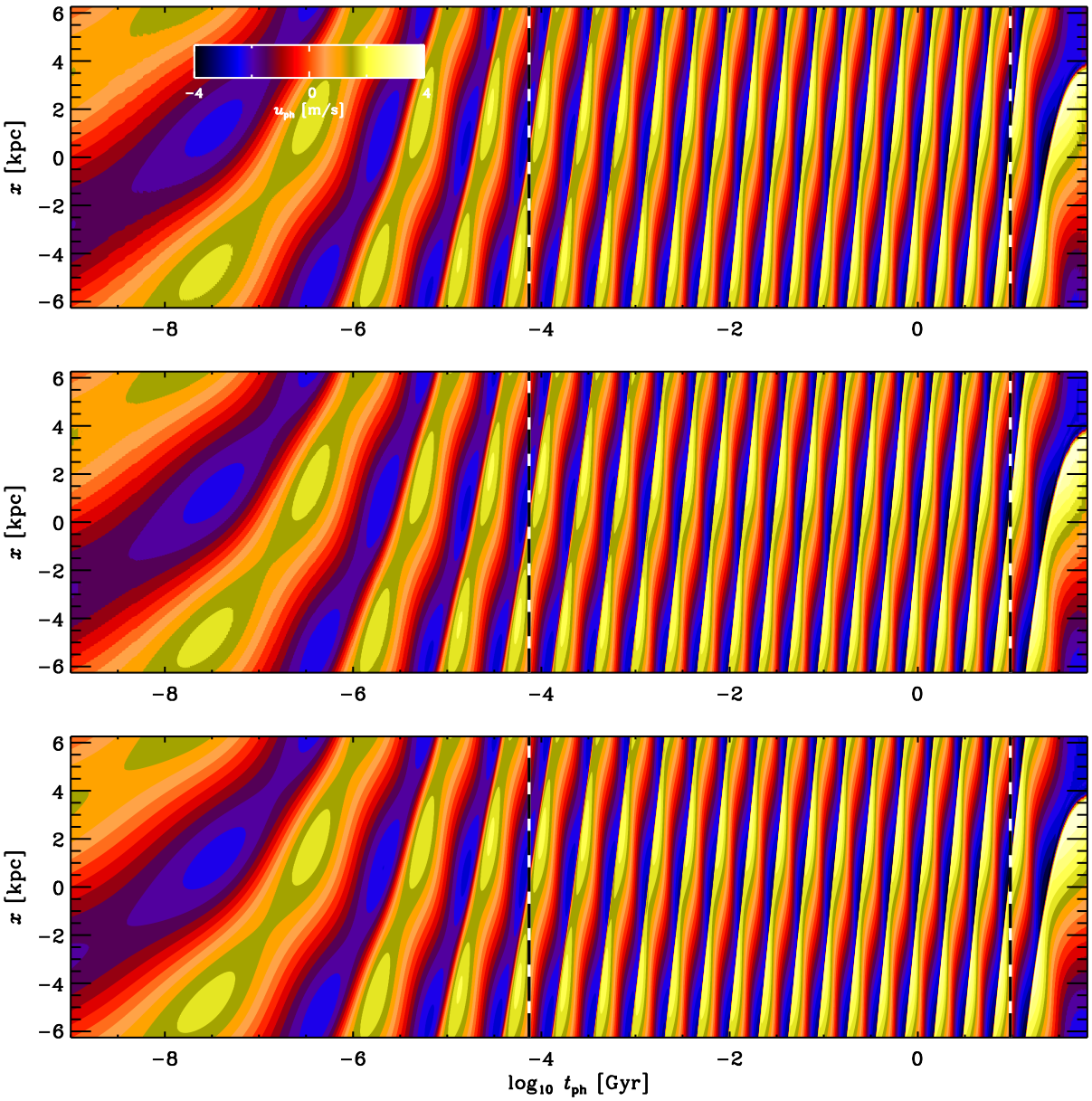

Figure 5: Space-time diagram of $u_{\rm ph}(t_{\rm ph}, x_{\rm ph})$, weighted with $a^{0.8}$ to compensate for the decay at late times for $n = 3/2$ (top) and $n = 2$ (bottom) with $k = 0.5\,{\rm kpc}^{-1}$ in both cases. The Mach number is 10^{-3}, and since $c_{3/2}(t_n) = {\rm const} = 1\,{\rm km/s}$, we used $u_{3/2}(0) = 10^{-3}\,{\rm km/s}$ in the first panel and $u_2(0) = 10^{-6}\,{\rm km/s}$ in the second. The vertical dashed-dotted lines denote the beginning and end of the matter-dominated phase.

7 Evolutionary tracks

Figure 11 shows evolutionary tracks in the $v_{\rm A}$–$\xi_{\rm M}$ diagram for Runs A–G. The lines for Runs A and B overlap, which might not be surprising, because they only differ in the starting point ($z_* = 4500$ and 10^6, respectively). On the other hand, both have been initialized with the same initial field with a spectrum that peaks at $k = 200\,k_0$. However, also Runs C and F overlap (green and dashed black lines), which

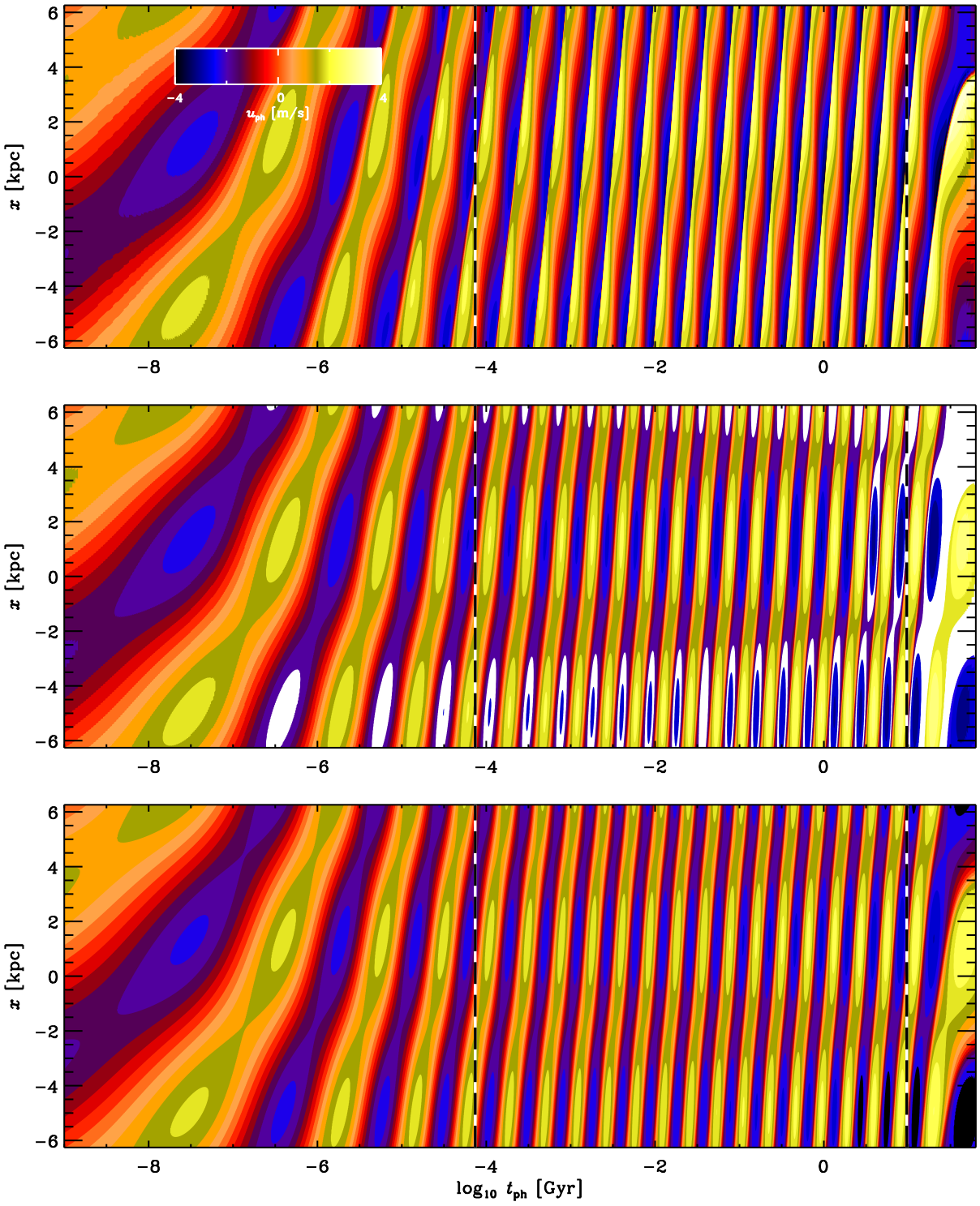

Figure 6: Similar to Figure 5, but for Alfven waves.

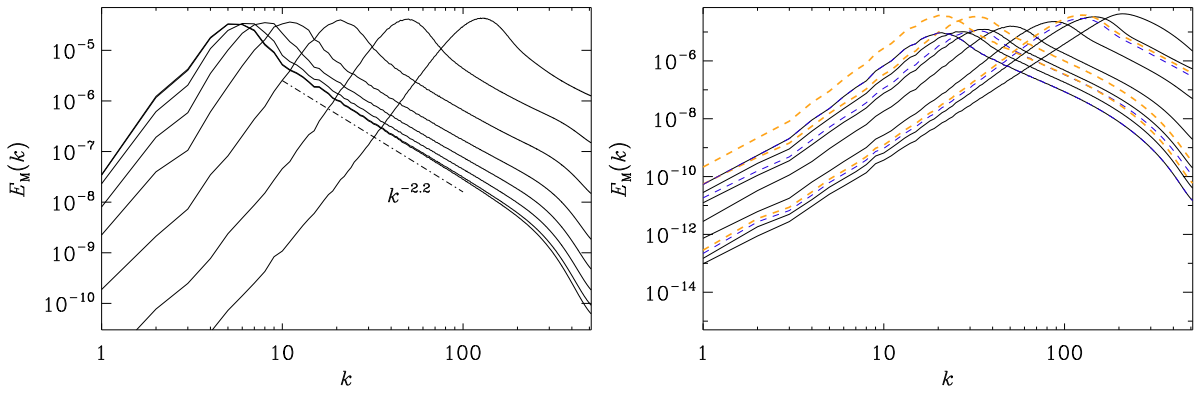

Figure 7: Left: spectra in supercomoving coordinates for $n = 3/2$ at $t = 0.5$, 4, 20, 60, 110, 165, 208, and 213 for 1024^3 mesh points, corresponding to $t_{\rm ph} = 3.6 \times 10^{-5}$, 5.3×10^{-5}, 2.1×10^{-4}, 3.3×10^{-3}, 6.4×10^{-2}, 1.3, and 58 Gyr for $\eta = \nu = 2 \times 10^{-6}$. Note that at high resolution, the peak amplitude does not decrease—even for the last few times well in the matter-dominated epoch starting with 3.3 Myr. This is surprising and suggests that the drag term is unimportant; we find $Ht \approx 2/3$ during the radiation-dominated epoch and larger terms up to 3 at later times. On the other hand, $\tilde{H}t$ varies from 0.03 to 800. Right: same, but for $n = 2$ (Run E) for $\eta = \nu = 2 \times 10^{-7}$. The orange lines denote the conformal times 34, 626, and 1238 (last time) (corresponding to physical times $t_{\rm ph} = 3.6 \times 10^{-5}$, 9.2×10^{-5}, and 3.0×10^{-4} Gyr), or $t_{\rm ph} = 36$, 92, and 300 kyr, but scaled by factors 1.3, 3, and 4.

only have in common the domain wavenumber $k_1 = 0.1$.

The lines $v_{\rm A} = \xi_{\rm M}/13.8\,{\rm Gyr}$ and $\xi_{\rm M}/400\,{\rm kyr}$ match the points with $t = 13.8\,{\rm Gyr}$ and $t = 400\,{\rm kyr}$. Such a relation was only expected to apply for conformal coordinates (left plot), but there the points are closer to $\xi_{\rm M}/10$ and $\xi_{\rm M}/3$, respectively.

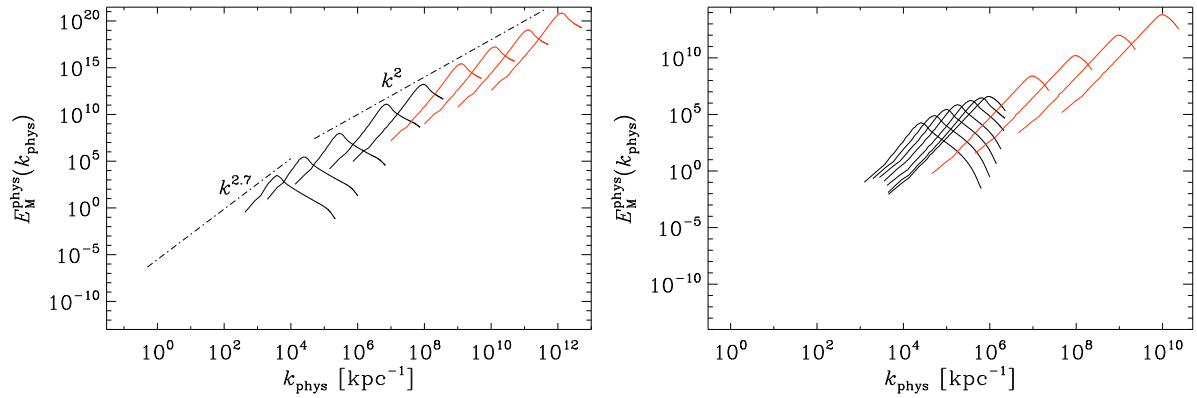

Figure 8: Left: physical spectra for a run with $n = 3/2$ starting at $z = 10^6$ at the times corresponding to
$t_{\rm ph} = 1.3 \times 10^{-9}$, 3.3×10^{-8}, 3.6×10^{-6}, 1.3×10^{-4}, 1.7×10^{-3}.
Right: physical spectra for a run with $n = 2$ starting at $z = 4500$ (default so far) at the times corresponding to $t_{\rm ph} = 1.2 \times 10^{-5}$, ... 1.4×10^{-4}.

Software and Data Availability. The source code used for the simulations of this study, the Pencil Code

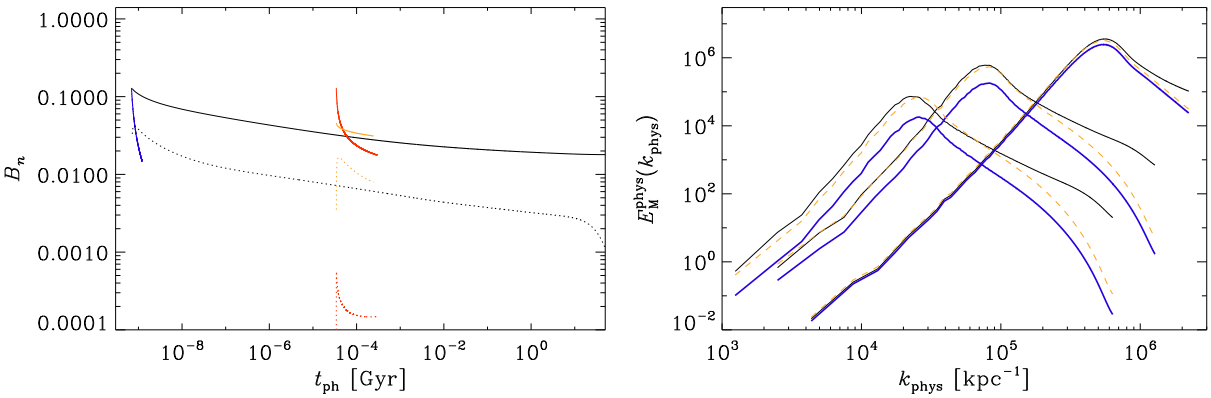

Figure 9: Left: Physical rms magnetic field, B/a^2, vs physical time for the run with $n = 3/2$ starting at $z = 10^6$ (black) with $\nu = \eta = 10^{-6}$. and two runs with $n = 2$ starting also at $z = 10^6$ (blue) or at $z = 4500$ (red), both with $\nu = \eta = 2 \times 10^{-7}$. Right: spectra in superconformal coordinates, but the three spectra from the left plot are highlighted in dashed blue and the upscaled version in dashed orange. Note that this correction factor makes the spectra stay at the same hight. Assuming that this correction accounts for numerical insufficiencies, this result supports the notion that the full inverse cascading would be preserved until matter domination.

(**?**), is freely available on `https://github.com/pencil-code`. The simulation setups and corresponding input and reduced output data are freely available on `http://norlx65.nordita.org/~brandenb/projects/InvCasc-to-MatterDom`.

$$c_n = a^{n_c}\, c_{\rm ref}. \tag{14}$$

$$\nu_n = a^{n_\nu}\, \nu_{\rm ref}. \tag{15}$$

$$\eta_n = a^{n_\eta}\, \eta_{\rm ref}. \tag{16}$$

Table 1: Scalings

n	n_c	$n_\nu = n_\eta$
1	-1	-0.5
2	$+1$	$+0.5$

8

The goal is to reproduce an $n = 3/2$ run with $n = 2$ and $n = 1$:

$$\nu_n = a^{n-3/2}\nu_{3/2},$$

$$\nu_2 = a^{1/2}\nu_{3/2},$$

$$\nu_1 = a^{-1/2}\nu_{3/2},$$

$$c_n^2 = a^{2(n-1)}\, c_{\rm s0,phys}^2,$$

$$c_2^2 = a^2\, c_{\rm s0,phys}^2,$$
$$c_1^2 = c_{\rm s0,phys}^2,$$
$$c_2 = a\, c_{\rm s0,phys},$$
$$c_1 = c_{\rm s0,phys},$$
$$\boldsymbol{u}_n = a^{n-1}\, \boldsymbol{u}_{\rm ph}. \tag{17}$$
$$\boldsymbol{u}_2 = a\, \boldsymbol{u}_{\rm ph}. \tag{18}$$
$$\boldsymbol{u}_{3/2} = a^{1/2}\, \boldsymbol{u}_{\rm ph}. \tag{19}$$
$$\boldsymbol{u}_1 = \boldsymbol{u}_{\rm ph}. \tag{20}$$
$$\boldsymbol{u}_2 = a^{1/2}\, \boldsymbol{u}_{3/2}. \tag{21}$$
$$\boldsymbol{u}_1 = a^{-1/2}\, \boldsymbol{u}_{3/2}. \tag{22}$$

So the Mach number remains unchanged.

References

Banerjee, R., & Jedamzik, K., "Evolution of cosmic magnetic fields: From the very early Universe, to recombination, to the present," *Phys. Rev. D* **70**, 123003 (2004).

Brandenburg, A., & Ntormousi, E., "Magnetic field amplification during a turbulent collapse," *Astrophys. J.* **990**, 223 (2025).

Brandenburg, A., Kahniashvili, T., & Tevzadze, A. G., "Nonhelical inverse transfer of a decaying turbulent magnetic field," *Phys. Rev. Lett.* **114**, 075001 (2015).

Jedamzik, K., & Pogosian, L., "Relieving the Hubble Tension with Primordial Magnetic Fields," *Phys. Rev. Lett.* **125**, 181302 (2020).

Jedamzik, K., Pogosian, L., & Zhao, G.-B., "
," *Comm. Phys.* **4**, 123–Why reducing the cosmic sound horizon alone can not fully resolve the Hubble tension (2021).

Jedamzik, K., Abel, T., & Ali-Haïmoud, Y., "Cosmic Recombination in the Presence of Primordial Magnetic Fields," *J. Cosm. Astrop. Phys.* **03**, 12 (2025).

Martel, H., & Shapiro, P. R., "A convenient set of comoving cosmological variables and their application," *Month. Not. Roy. Astron. Soc.* **297**, 467–485 (1998).

$Header: /var/cvs/brandenb/tex/teach/COSMOMAG26/5_during_recombination/notes.tex,v 1.5 2026/01/16 10:18:05 brandenb Exp $

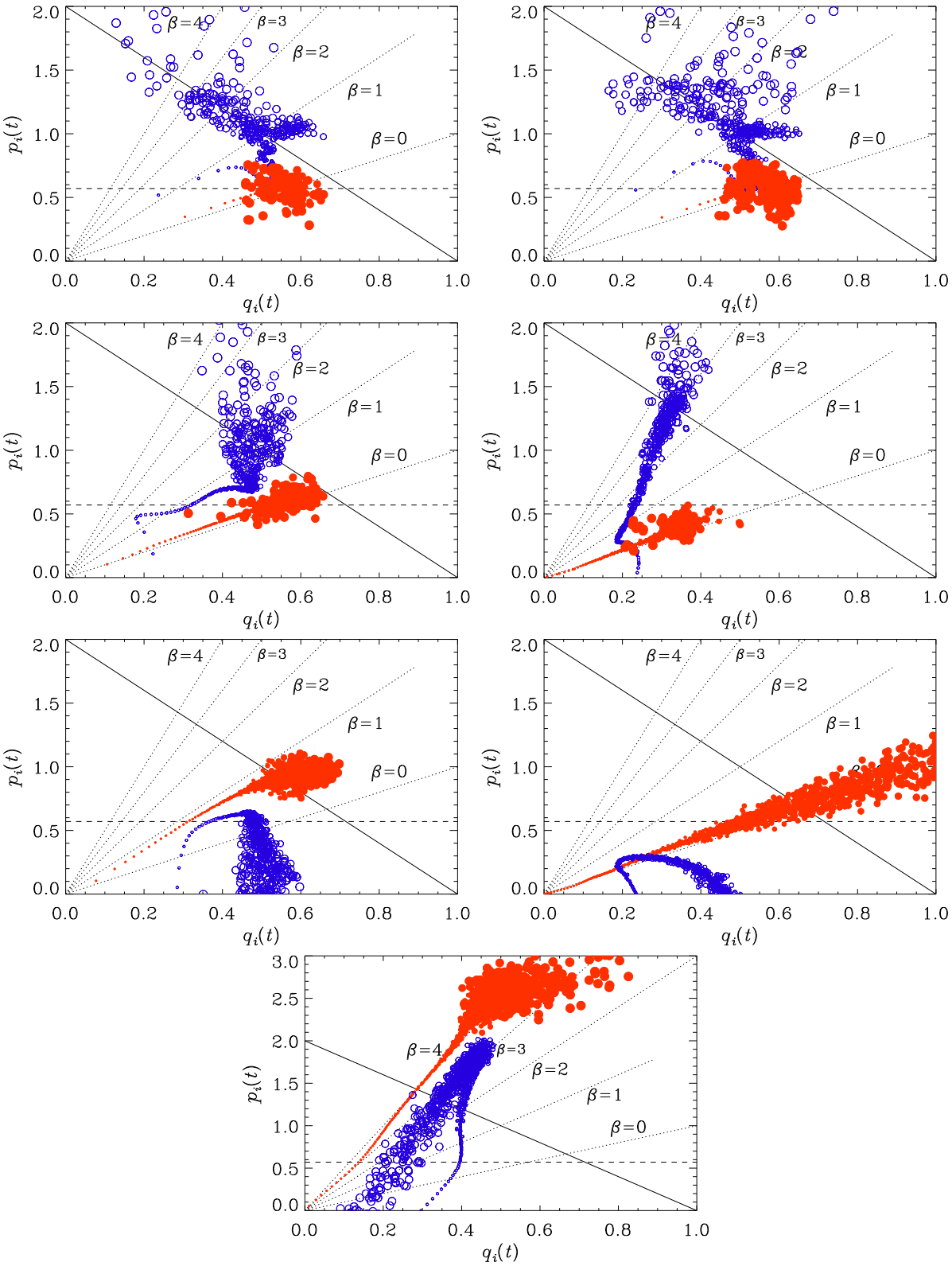

Figure 10: *pq* diagrams for Runs A–G.

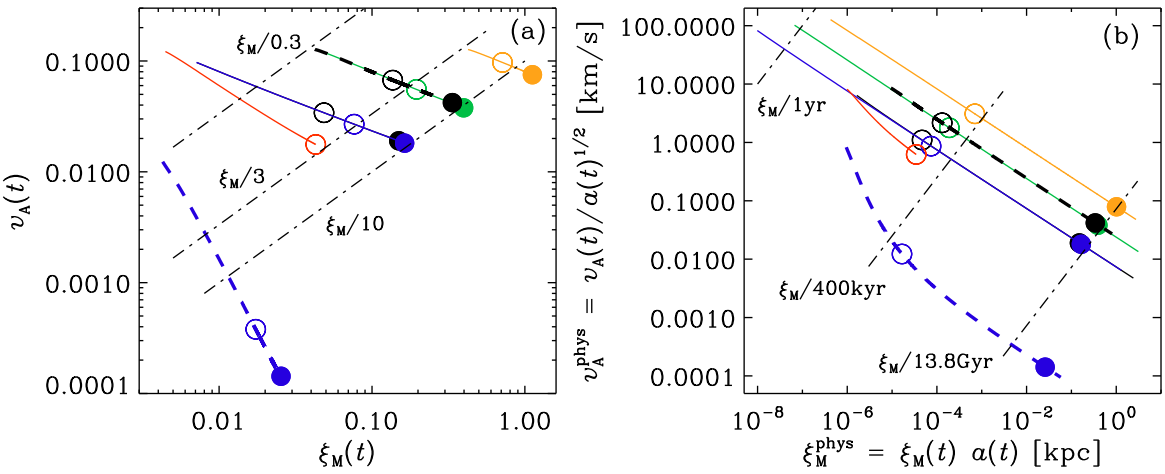

Figure 11: v_A–ξ_M diagram for the same 7 runs (black, blue, green, orange, red, black dashed, blue dashed) as in Figure 10 for (a) conformal and (b) physical variables. Note that in (a), the solid blue and black lines for Runs A and B overlap. The filled (open) symbols denote the times $t = 13.8\,\mathrm{Gyr}$ and 400 kyr, respectively.